Optimal Frequency for Wireless Power Transmission over Dispersive Tissue

Ada S. Y. Poon*, Stephen O'Driscoll†, and Teresa H. Meng‡

March 8, 2008

Abstract

Conventional wisdom in wireless power transmission over dispersive tissue tends to operate at frequency less than 10 MHz due to tissue absorption loss. In the past half century, analyses, circuit design techniques, and prototype implementation of wireless power link for medical implants are developed entirely in this low-frequency range. This paper re-examines the optimal frequency for the operation of these wireless interfaces. It carries out full-wave analysis and shows that the optimal frequency is about 2 order of magnitude higher than the conventional wisdom. Consequently, the efficiency can be improved by 30 dB by operating at the optimal frequency. Alternatively, the receive area can be reduced by 100 times for a given efficiency.

1 Introduction

Between 1960s and 1980s, several detailed studies of wireless power transmission for medical implants were carried out [1–5]. They focused on the operation at frequencies below 20 MHz. Transformer model and quasi-static analysis were therefore used in these studies. Based on their results, circuit design techniques including tuning configurations [4,6–11] and geometry

*Ada S. Y. Poon is with the Department of Electrical and Computer Engineering, University of Illinois at Urbana-Champaign, poon@uiuc.edu

†Stephen O'Driscoll is with the Department of Electrical Engineering, Stanford University, stiofan@stanford.edu

‡Teresa H. Meng is with the Department of Electrical Engineering, Stanford University, thm@stanford.edu

optimization [12] were developed in the late 1970s through 1990s. All these design techniques were based on the transformer model and the principle of inductive coupling. In the past ten years, some of these techniques have been applied to the implementation of highly integrated implantable microsystems [13, 14]. Their transmission frequencies are all below 10 MHz. Presumably, throughout the development of wireless power transmission over body tissue, the optimal frequency range is below 10 MHz. However, we cannot find any vigorous proof of this rule of thumb.

The choice of the transmission frequency is a trade-off between miniaturization and tissue absorption. The amount of received power increases with increasing rate of change of the transmitting field, that is, higher transmission frequency delivers more received power. In other words, we can use a smaller receiver at higher frequency for a fixed received power. However, body tissue is dispersive. Higher frequency incurs more tissue absorption. Consequently, there is an optimal transmission frequency on the power transfer efficiency. Our objectives are to find this optimal frequency, and to investigate how the optimal frequency affects by the depth of the implant inside the body, the layered structure of tissue, and the dimension of the transmitter.

To ensure our derivation on the power transfer efficiency is valid over a wide frequency range, we need to devise the power transmission model that is not based on the transformer model. Because the transformer model is a low-frequency approximation which is not adequate to conclude the power transfer efficiency at higher frequencies. Indeed, we will show that the conclusion draw from this low-frequency approximation does not favor the operation at higher frequencies.

Based on the devised model, we will first consider a dispersive homogeneous medium. We carry out full-wave analysis and show that the optimal transmission frequency is in the GHz-range for typical biological tissue dielectric properties. The frequency is at least 2 order of magnitude higher than the conventional wisdom. Furthermore, we show that the optimal power transfer efficiency is inversely proportional to the cube of the depth of implant inside body. This implies that the regime for optimal power transmission is in between the far field and the near field.

Our analysis in the homogeneous medium brings out that the dispersiveness of body tissue is not as worse as conventional wisdom believed. Next, we will include the inhomogeneous nature of body tissue and investigate its effect on the optimal frequency. Scattering from tissue interfaces reduces the optimal frequency. However, the optimal frequency remains in the GHz-range. It is relatively invariant with the implant depth and the orientation of the receiver. Scattering also reduces the optimal efficiency by almost an order of magnitude. However, the efficiency remains inversely proportional to the cube of the implant depth.

In our analyses, we consider the scenario where the dimension of the implantable device is small relative to the depth of the implant inside the body, for example, a 2-mm width coil at a depth of 2 cm. Therefore, we use point sources to model both the transmitter and the receiver. Finally, we will verify this point-source approximation by full-wave electromagnetic simulation using finite sized sources. We use Zeland IE3D [15] which is a solver based on method of moment. The simulated results match well with the theoretical ones. In addition, we also investigate how the transmitter dimension affects the optimal frequency. Larger dimension reduces the optimal frequency. For a practical dimension of the transmitter, the optimal frequency is in the sub-GHz range. Compared with the conventional wisdom, the optimal frequency is about 2 order of magnitude higher. For a fixed received power, the receive area can be reduced by 10^6 times. For a fixed receive area, the efficiency can be improved by 30 dB including scattering loss. For a fixed efficiency, the receive area can be reduced by 100 times.

The rest of the paper is organized as follows. Section 2 presents the power transmission model. Section 3 derives the optimal transmission frequency in dispersive homogeneous medium. Section 4 extends the analysis to inhomogeneous layered medium. Section 5 verifies the analytical results and the numerical examples by full-wave electromagnetic simulations. Finally, we will conclude this paper in Section 6.

In the following, we use boldface letters for vectors and boldface letters with a bar $\bar{\mathbf{G}}$ for matrices. For a vector $\mathbf{v}$, v denotes its magnitude and $\hat{\mathbf{v}}$ is a unit vector denoting its direction. $(\cdot)^*$ and $(\cdot)^\dagger$ denote the conjugate and the conjugate-transpose operations respectively. For a complex number z, $\mathrm{Re}\, z$ and $\mathrm{Im}\, z$ denote the real and the imaginary parts respectively. The relation $f(x) \sim g(x)$ means that $\lim_{x\to\infty} \frac{f(x)}{g(x)}$ is a constant.

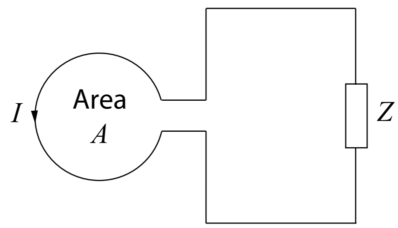

Figure 1: A receive current loop connected to a load Z.

2 Modeling of Power Transmission

As current loops are usually used in the wireless powering of implants, it is more convenient to consider magnetic current density as sources. In addition, we assume that all fields and sources have a time dependence $e^{-i\omega t}$. Electromagnetic fields due to the transmit magnetic current density $\mathbf{J}_{m,1}(\mathbf{r})$ and the receive magnetic current density $\mathbf{J}_{m,2}(\mathbf{r})$ in a medium of relative permittivity ϵ_r and conductivity σ satisfy

$$\nabla \times \mathbf{H} = -i\omega\epsilon_0\epsilon_r\mathbf{E} + \sigma\mathbf{E} \tag{1a}$$

$$\nabla \times \mathbf{E} = i\omega\mu_0\mathbf{H} - \mathbf{J}_{m,1} - \mathbf{J}_{m,2} \tag{1b}$$

Substituting them into the Poynting vector yields

$$\nabla \cdot (\mathbf{E} \times \mathbf{H}^*) = i\omega\mu_0|\mathbf{H}|^2 - i\omega\epsilon_0\epsilon_r|\mathbf{E}|^2 - \sigma|\mathbf{E}|^2 - \mathbf{H}^* \cdot \mathbf{J}_{m,1} - \mathbf{H}^* \cdot \mathbf{J}_{m,2} \tag{2}$$

Rearranging terms, we relate the transmitted power to the received power plus losses:

$$-\mathbf{H}^* \cdot \mathbf{J}_{m,1} = \nabla \cdot (\mathbf{E} \times \mathbf{H}^*) + i\omega\mu_0|\mathbf{H}|^2 - i\omega\epsilon_0\epsilon_r^*|\mathbf{E}|^2 + \sigma|\mathbf{E}|^2 + \mathbf{H}^* \cdot \mathbf{J}_{m,2} \tag{3}$$

The term on the left is the complex transmitted power. On the right, $\nabla \cdot (\mathbf{E} \times \mathbf{H}^*)$ is the radiation loss; $\omega\epsilon_0 \operatorname{Im}\epsilon_r|\mathbf{E}|^2$ is the dielectric loss; $\sigma|\mathbf{E}|^2$ is the induced-current loss; and $\mathbf{H}^* \cdot \mathbf{J}_{m,2}$ is the complex received power. We define the power transfer efficiency η as the ratio of real received power to tissue absorption (dielectric loss plus induced-current loss), that is,

$$\eta := \frac{P_r}{P_l} = \frac{\operatorname{Re}\int \mathbf{H}^*(\mathbf{r}) \cdot \mathbf{J}_{m,2}(\mathbf{r})\, d\mathbf{r}}{\int \left[\omega\epsilon_0 \operatorname{Im}\epsilon_r(\mathbf{r}) + \sigma(\mathbf{r})\right] \left|\mathbf{E}(\mathbf{r})\right|^2 d\mathbf{r}} \tag{4}$$

The integration in the numerator is over the received volume while the integration in the denominator is over the tissue volume.

As $\mathbf{J}_{m,2}(\mathbf{r})$ is induced by $\mathbf{H}(\mathbf{r})$ over the received volume, we want to relate $\mathbf{J}_{m,2}(\mathbf{r})$ to $\mathbf{H}(\mathbf{r})$. Consider the receive current loop shown in Fig. 1. The total magnetic flux incident on the receive loop is $\mu_0 \int_{\text{rx loop}} \mathbf{H}(\mathbf{r}) \cdot \hat{\mathbf{n}}\, ds$ where $\hat{\mathbf{n}}$ denotes the orientation of the receive loop. The rate of change of this total magnetic flux yields the induced emf. This induced emf is the voltage across Z. The current is therefore given by

$$I = \frac{i\omega\mu_0}{Z} \int_{\text{rx loop}} \mathbf{H}(\mathbf{r}) \cdot \hat{\mathbf{n}}\, ds \tag{5}$$

The direction of $\mathbf{J}_{m,2}(\mathbf{r})$ is $\hat{\mathbf{n}}$. From definition, its magnitude $J_{m,2}(\mathbf{r})$ relates to the induced magnetic moment density as

$$\begin{aligned} J_{m,2}(\mathbf{r}) &= -i\omega\mu_0 I A && \text{(6a)} \\ &= \frac{\omega^2\mu_0^2 A}{Z} \int_{\text{rx loop}} \mathbf{H}(\mathbf{r}) \cdot \hat{\mathbf{n}}\, ds && \text{(6b)} \end{aligned}$$

We consider area-constrained implantable devices so we model the receiver as a point source. Thus, we have

$$J_{m,2}(\mathbf{r}) = \frac{\omega^2\mu_0^2 A^2}{Z}\, \mathbf{H}(-\hat{\mathbf{z}}d_2) \cdot \hat{\mathbf{n}}\, \delta(\mathbf{r} + \hat{\mathbf{z}}d) \tag{7}$$

where $-\hat{\mathbf{z}}d$ is the location of the receiver. Substituting it into (4) yields

$$\eta = \frac{\omega^2\mu_0^2 A^2/Z \left|\mathbf{H}(-\hat{\mathbf{z}}d) \cdot \hat{\mathbf{n}}\right|^2}{\int \left[\omega\epsilon_0 \operatorname{Im}\epsilon_r(\mathbf{r}) + \sigma(\mathbf{r})\right] \left|\mathbf{E}(\mathbf{r})\right|^2 d\mathbf{r}} \tag{8}$$

The power transfer efficiency is now in terms of the incident magnetic field at $-\hat{\mathbf{z}}d$ and the electric field over the tissue volume. In the following, we will first derive these fields due to a transmit vector point source in a dispersive homogeneous medium and study how the efficiency varies with frequency. Then, we will replace the homogeneous medium with a layered tissue model, and carry out the same study. Finally, we will replace the point sources with finite coils, and carry out electromagnetic simulation to verify the analytical results based on point sources.

3 Vector Point Source in Homogeneous Medium

We model the transmitter as a vector point source. The magnetic and the electric fields can be represented by a basis set consisting of 6 vector elements:

$$\mathbf{M}_{1m}(\mathbf{r}) = \nabla \times \left[\mathbf{r} h_n^{(1)}(kr) Y_{nm}(\theta,\phi)\right], \quad m=-1,0,1 \tag{9a}$$

$$\mathbf{N}_{1m}(\mathbf{r}) = \frac{1}{k}\nabla \times \nabla \times \left[\mathbf{r} h_n^{(1)}(kr) Y_{nm}(\theta,\phi)\right], \quad m=-1,0,1 \tag{9b}$$

where $k^2 = \omega^2\mu_0\epsilon_0\big(\epsilon_r + i\frac{\sigma}{\omega\epsilon_0}\big)$. These basis elements correspond to the lowest order modes in spherical multipole expansion of the daydic Green's functions in homogeneous medium. Specifically, $\mathbf{N}_{10}(\mathbf{r})$ and $\mathbf{M}_{10}(\mathbf{r})$ are the respective magnetic field and electric field due to an infinitesimal current loop oriented along the z-axis; $\frac{1}{\sqrt{2}}\mathbf{N}_{1,-1}(\mathbf{r}) - \frac{1}{\sqrt{2}}\mathbf{N}_{1,1}(\mathbf{r})$ and $\frac{1}{\sqrt{2}}\mathbf{M}_{1,-1}(\mathbf{r}) - \frac{1}{\sqrt{2}}\mathbf{M}_{1,1}(\mathbf{r})$ are the respective magnetic field and electric field due to a current loop oriented along the x-axis; and $\frac{i}{\sqrt{2}}\mathbf{N}_{1,-1}(\mathbf{r}) + \frac{i}{\sqrt{2}}\mathbf{N}_{1,1}(\mathbf{r})$ and $\frac{i}{\sqrt{2}}\mathbf{M}_{1,-1}(\mathbf{r}) + \frac{i}{\sqrt{2}}\mathbf{M}_{1,1}(\mathbf{r})$ are the respective magnetic field and electric field due to a current loop oriented along the y-axis. As the scattered field due to $\mathbf{J}_{m2}(\mathbf{r})$ is much weaker than the incident field due to $\mathbf{J}_{m,1}(\mathbf{r})$, the magnetic and the electric fields can be expressed as

$$\mathbf{H}(\mathbf{r}) = -k^3\left[\alpha_{-1}\mathbf{N}_{1,-1}(\mathbf{r}) + \alpha_0\mathbf{N}_{1,0}(\mathbf{r}) + \alpha_1\mathbf{N}_{1,1}(\mathbf{r})\right] \tag{10a}$$

$$\mathbf{E}(\mathbf{r}) = -i\omega\mu_0 k^2\left[\alpha_{-1}\mathbf{M}_{1,-1}(\mathbf{r}) + \alpha_0\mathbf{M}_{1,0}(\mathbf{r}) + \alpha_1\mathbf{M}_{1,1}(\mathbf{r})\right] \tag{10b}$$

where $(\alpha_{-1}, \alpha_0, \alpha_1) \in \mathcal{C}^3$ denotes the orientation of the transmit coil.

Now, the received power and the tissue absorption can be written in terms of α_m's. For a given orientation of the receive coil $\hat{\mathbf{n}}$, we will first derive the optimal power transfer efficiency that maximizes over all possible orientations of the transmit coil, α_m's. Then, we will analyze this optimal power transfer efficiency under different approximations and dielectric models.

3.1 Optimal Power Transfer Efficiency

Suppose the transmitter is at the origin, the tissue volume spans $z < -d_1$, and the receiver is at $-d_2$. Then, the tissue absorption is

$$P_l = \frac{\omega\mu_0|k|^4\,\mathrm{Im}\,k^2}{2}\int_{\text{tissue}}\left|\alpha_{-1}\mathbf{M}_{1,-1}(\mathbf{r}) + \alpha_0\mathbf{M}_{1,0}(\mathbf{r}) + \alpha_1\mathbf{M}_{1,1}(\mathbf{r})\right|^2 d\mathbf{r} \tag{11}$$

The symmetry in ϕ of the tissue volume implies that the cross terms are zero. Therefore, we have

$$P_l = \frac{\omega\mu_0|k|^4 \operatorname{Im} k^2}{2} \int_{\text{tissue}} |\alpha_{-1}|^2 \big|\mathbf{M}^{(3)}_{1,-1}(\mathbf{r})\big|^2 + |\alpha_0|^2 \big|\mathbf{M}^{(3)}_{1,0}(\mathbf{r})\big|^2 + |\alpha_1|^2 \big|\mathbf{M}^{(3)}_{1,1}(\mathbf{r})\big|^2 \, d\mathbf{r} \tag{12}$$

For the received power, we expand the orientation of the receive coil as

$$\hat{\mathbf{n}} = \beta_{-1} \frac{\mathbf{N}_{1,-1}(-\hat{\mathbf{z}}d_2)}{|\mathbf{N}_{1,-1}(-\hat{\mathbf{z}}d_2)|} + \beta_0 \frac{\mathbf{N}_{1,0}(-\hat{\mathbf{z}}d_2)}{|\mathbf{N}_{1,0}(-\hat{\mathbf{z}}d_2)|} + \beta_1 \frac{\mathbf{N}_{1,1}(-\hat{\mathbf{z}}d_2)}{|\mathbf{N}_{1,1}(-\hat{\mathbf{z}}d_2)|} \tag{13}$$

for some β_m's satisfying $|\beta_{-1}|^2 + |\beta_0|^2 + |\beta_1|^2 = 1$. The directions of $\mathbf{N}_{1,-1}(-\hat{\mathbf{z}}d_2)$ and $\mathbf{N}_{1,1}(-\hat{\mathbf{z}}d_2)$ are orthogonal and lie on the xy-plane, while the direction of $\mathbf{N}_{1,0}(-\hat{\mathbf{z}}d_2)$ is $\hat{\mathbf{z}}$. The received power becomes

$$P_r = \frac{\omega^2\mu_0^2|k|^6 A^2}{2Z} \Big| \alpha_{-1}\beta^*_{-1} \big|\mathbf{N}_{1,-1}(-\hat{\mathbf{z}}d_2)\big| + \alpha_0\beta^*_0 \big|\mathbf{N}_{1,0}(-\hat{\mathbf{z}}d_2)\big| + \alpha_1\beta^*_1 \big|\mathbf{N}_{1,1}(-\hat{\mathbf{z}}d_2)\big| \Big|^2 \tag{14}$$

Now, we maximize the power transfer efficiency over all possible orientations of the transmit coil. The optimal power transfer efficiency is given by

$$\eta_{opt} = \frac{\omega\mu_0|k|^2 A^2}{Z \operatorname{Im} k^2} \Big[\frac{\big|\beta_{-1}\mathbf{N}_{1,-1}(-\hat{\mathbf{z}}d_2)\big|^2}{\int_{\text{tissue}} \big|\mathbf{M}_{1,-1}(\mathbf{r})\big|^2 \, d\mathbf{r}} + \frac{\big|\beta_0\mathbf{N}_{1,0}(-\hat{\mathbf{z}}d_2)\big|^2}{\int_{\text{tissue}} \big|\mathbf{M}_{1,0}(\mathbf{r})\big|^2 \, d\mathbf{r}} + \frac{\big|\beta_1\mathbf{N}_{1,1}(-\hat{\mathbf{z}}d_2)\big|^2}{\int_{\text{tissue}} \big|\mathbf{M}_{1,1}(\mathbf{r})\big|^2 \, d\mathbf{r}} \Big] \tag{15}$$

and the corresponding orientation of the transmit coil is

$$\alpha_m = \frac{\big|\mathbf{N}_{1,m}(-\hat{\mathbf{z}}d_2)\big|}{\int_{\text{tissue}} \big|\mathbf{M}_{1,m}(\mathbf{r})\big|^2 \, d\mathbf{r}} \beta_m, \quad m = -1, 0, 1 \tag{16}$$

The proof is included in Appendix A. Furthermore, from definitions in (9), we obtain

$$\begin{aligned}
\int_{\text{tissue}} \big|\mathbf{M}_{1,-1}(\mathbf{r})\big|^2 \, d\mathbf{r} = \int_{\text{tissue}} \big|\mathbf{M}_{1,1}(\mathbf{r})\big|^2 \, d\mathbf{r} \\
&= \frac{e^{-2k_I d_1}}{16|k|^4 d_1} \Big[9 - 14k_I d_1 + 2k_I^2 d_1^2 - 4k_I^3 d_1^3 + 8|k|^2 d_1^2 \big(\frac{1}{k_I d_1} - \frac{1}{4} + \frac{k_I d_1}{2} \big) \Big] \\
&\quad + \frac{\operatorname{Ei}(-2k_I d_1)}{4|k|^4 d_1} \Big[|k|^2 d_1^2 \big(3 + 2k_I^2 d_1^2\big) - 2k_I^2 d_1^2 \big(3 + k_I^2 d_1^2\big) \Big]
\end{aligned} \tag{17a}$$

$$\begin{aligned}
\int_{\text{tissue}} \big|\mathbf{M}_{1,0}(\mathbf{r})\big|^2 \, d\mathbf{r} &= \frac{e^{-2k_I d_1}}{8|k|^4 d_1} \Big[3 - 10k_I d_1 - 2k_I^2 d_1^2 + 4k_I^3 d_1^3 + 4|k|^2 d_1^2 \big(\frac{1}{k_I d_1} + \frac{1}{2} - k_I d_1 \big) \Big] \\
&\quad + \frac{\operatorname{Ei}(-2k_I d_1)}{2|k|^4 d_1} \Big[|k|^2 d_1^2 \big(3 - 2k_I^2 d_1^2\big) - 2k_I^2 d_1^2 \big(3 - k_I^2 d_1^2\big) \Big]
\end{aligned} \tag{17b}$$

and

$$\begin{aligned}
\big|\mathbf{N}_{1,-1}(-\hat{\mathbf{z}}d_2)\big|^2 = \big|\mathbf{N}_{1,1}(-\hat{\mathbf{z}}d_2)\big|^2 \\
&= \frac{3e^{-2k_I d_2}}{4\pi|k|^6 d_2^6} \Big[1 - |k|^2 d_2^2 + |k|^4 d_2^4 + 2k_I d_2 \big(1 + 2k_I d_2 + |k|^2 d_2^2\big) \Big]
\end{aligned} \tag{18a}$$

$$\big|\mathbf{N}_{1,0}(-\hat{\mathbf{z}}d_2)\big|^2 = \frac{3e^{-2k_I d_2}}{\pi|k|^6 d_2^6} (1 + 2k_I d_2 + |k|^2 d_2^2) \tag{18b}$$

where $k_I = \operatorname{Im} k$ and $\operatorname{Ei}(\cdot)$ is the exponential integral function.

From (16), it is not necessary to orient the transmit coil along the same direction as the receive coil for maximum power delivery. There are certain directions where the tissue absorption is less, while there are some directions where the received power is more. The optimal orientation is a trade-off between them and this trade-off varies with frequency. This is the reason why we study the variation of the efficiency with frequency that is optimized over all possible transmit orientation.

3.2 Static and Quasi-static Approximations

At DC, $\omega = 0$, and therefore $|k| = k_I = 0$ and $\operatorname{Im} k^2/(\omega\mu_0) = \sigma$. We have

$$\frac{|k|^2\left|\mathbf{N}_{1,-1}(-\hat{\mathbf{z}}d_2)\right|^2}{\int_{\text{tissue}}\left|\mathbf{M}_{1,-1}(\mathbf{r})\right|^2 d\mathbf{r}} = \frac{|k|^2\left|\mathbf{N}_{1,1}(-\hat{\mathbf{z}}d_2)\right|^2}{\int_{\text{tissue}}\left|\mathbf{M}_{1,1}(\mathbf{r})\right|^2 d\mathbf{r}} = \frac{4d_1}{3\pi d_2^6} \tag{19a}$$

$$\frac{|k|^2\left|\mathbf{N}_{1,0}(-\hat{\mathbf{z}}d_2)\right|^2}{\int_{\text{tissue}}\left|\mathbf{M}_{1,0}(\mathbf{r})\right|^2 d\mathbf{r}} = \frac{8d_1}{\pi d_2^6} \tag{19b}$$

The static optimal power transfer efficiency is

$$\eta_{opt,0} = \frac{4d_1 A^2/Z}{3\pi\sigma d_2^6}\left(|\beta_{-1}|^2 + 6|\beta_0|^2 + |\beta_1|^2\right) \tag{20}$$

The optimal efficiency is independent of frequency. It is maximized when $|\beta_0| = 1$ and $|\beta_{-1}| = |\beta_1| = 0$, that is, the receive coil is oriented along $\hat{\mathbf{z}}$.

At low frequency, the displacement current $-i\omega\epsilon_0\epsilon_r\mathbf{E}$ is small. Quasi-static approximation neglects this current which is equivalent to setting ϵ_r equal to 0. The wavenumber is then given by

$$k = \sqrt{\frac{\omega\mu_0\sigma}{2}}(1+i) \tag{21}$$

This yields

$$|k|^2 = 2k_I^2 = \omega\mu_0\sigma$$

Suppose d_1 is much smaller than the skin depth, that is, $k_I d_1 \ll 1$. Then,

$$\begin{aligned}\frac{|k|^2\left|\mathbf{N}_{1,-1}(-\hat{\mathbf{z}}d_2)\right|^2}{\int_{\text{tissue}}\left|\mathbf{M}_{1,-1}(\mathbf{r})\right|^2 d\mathbf{r}} &= \frac{|k|^2\left|\mathbf{N}_{1,1}(-\hat{\mathbf{z}}d_2)\right|^2}{\int_{\text{tissue}}\left|\mathbf{M}_{1,1}(\mathbf{r})\right|^2 d\mathbf{r}} \\ &= \frac{4d_1}{3\pi d_2^4}\left(|k|^2 d_2^2 + \sqrt{2}|k|d_2 + 1\right)|k|^2 e^{-2k_I d_2} + o\left(|k|^2 e^{-2k_I d_2}\right)\end{aligned} \tag{22a}$$

$$\frac{|k|^2\left|\mathbf{N}_{1,0}(-\hat{\mathbf{z}}d_2)\right|^2}{\int_{\text{tissue}}\left|\mathbf{M}_{1,0}(\mathbf{r})\right|^2 d\mathbf{r}} = \frac{8d_1}{\pi d_2^4}|k|^2 e^{-2k_I d_2} + o\left(|k|^2 e^{-2k_I d_2}\right) \tag{22b}$$

as $\omega \to \infty$. The quasi-static optimal efficiency is

$$\eta_{opt} = \frac{4d_1 A^2/Z}{3\pi\sigma d_2^4}\Big[6|\beta_0|^2 + \big(|k|^2 d_2^2 + \sqrt{2}|k|d_2 + 1\big)\big(|\beta_{-1}|^2 + |\beta_1|^2\big)\Big]|k|^2 e^{-2k_I d_2} + o\big(|k|^2 e^{-2k_I d_2}\big) \tag{23}$$

In terms of the static optimal efficiency,

$$\eta_{opt} = \eta_{opt,0}\, e^{-2k_I d_2} \cdot |k|^2 d_2^2\Big[1 + \frac{|\beta_{-1}|^2 + |\beta_1|^2}{|\beta_{-1}|^2 + 6|\beta_0|^2 + |\beta_1|^2}\big(|k|^2 d_2^2 + \sqrt{2}|k|d_2\big)\Big] + o\big(|k|^2 e^{-2k_I d_2}\big) \tag{24}$$

As $k_I \propto \sqrt{\omega}$, the optimal efficiency decreases exponentially with $\sqrt{\omega}$. Therefore, it is worse to operate at higher frequencies than at DC. We believed that this is also the source for the conventional wisdom of operating below 10 MHz.

3.3 Full-wave Analysis without Relaxation Loss

Including the displacement current, the wavenumber becomes

$$k = \omega\sqrt{\mu_0\epsilon_0\epsilon_r} + i\frac{\sigma}{2}\sqrt{\frac{\mu_0}{\epsilon_0\epsilon_r}} + o(1) \tag{25}$$

as $\omega \to \infty$. This yields

$$k_I = \frac{\sigma}{2}\sqrt{\frac{\mu_0}{\epsilon_0\epsilon_r}} + o(1) \qquad |k| = \omega\sqrt{\mu_0\epsilon_0\epsilon_r} + o(\omega) \tag{26}$$

Now k_I is asymptotically invariant with frequency. Similarly, we assume that d_1 is much smaller than the skin depth, that is, $k_I d_1 \ll 1$. Then

$$\frac{|k|^2\big|\mathbf{N}_{1,-1}(-\hat{\mathbf{z}}d_2)\big|^2}{\int_{\text{tissue}}\big|\mathbf{M}_{1,-1}(\mathbf{r})\big|^2\, d\mathbf{r}} = \frac{|k|^2\big|\mathbf{N}_{1,1}(-\hat{\mathbf{z}}d_2)\big|^2}{\int_{\text{tissue}}\big|\mathbf{M}_{1,1}(\mathbf{r})\big|^2\, d\mathbf{r}} = \frac{3k_I e^{-2k_I d_2}}{2\pi d_2^4}\big(|k|^2 d_2^2 + 2k_I d_2 - 1\big) + o(1) \tag{27a}$$

$$\frac{|k|^2\big|\mathbf{N}_{1,0}(-\hat{\mathbf{z}}d_2)\big|^2}{\int_{\text{tissue}}\big|\mathbf{M}_{1,0}(\mathbf{r})\big|^2\, d\mathbf{r}} = \frac{6k_I e^{-2k_I d_2}}{\pi d_2^4} + o(1) \tag{27b}$$

as $\omega \to \infty$. The optimal efficiency is

$$\eta_{opt} = \frac{3k_I e^{-2k_I d_2} A^2/Z}{2\pi\sigma d_2^4}\Big[4|\beta_0|^2 + \big(|k|^2 d_2^2 + 2k_I d_2 - 1\big)\big(|\beta_{-1}|^2 + |\beta_1|^2\big)\Big] + o(1) \tag{28}$$

In contrast to the optimal efficiency obtained from quasi-static analysis, the efficiency from full-wave analysis increases with frequency asymptotically. This difference in the conclusions illustrates that current analysis techniques for wireless power transmission over body tissue are not adequate.

3.4 Full-wave Analysis including Relaxation Loss

The efficiency would not increase indefinitely with frequency. At high frequency, there are loss mechanisms other than induced current. The dominant mechanism is the relaxation loss [16]. Consequently, there will be an optimal transmission frequency. We are interested in finding where it is, in the MHz-range or in the GHz-range. If it is in the MHz-range, quasi-static approximation would be sufficient. On the other hand, if it is in the GHz-range, new analysis and new design techniques will be needed. To address this question, a relaxation model is required.

From (3), the dielectric loss $\omega\epsilon_0 \operatorname{Im}\epsilon_r|\mathbf{E}|^2$ encapsulates the relaxation loss. As $\operatorname{Im}\epsilon_r \neq 0$, Kramers-Kronig relations [17, Section 7.10] ensure that ϵ_r varies with frequency. Therefore, dielectric relaxation is often modeled by a frequency-dependent relative permittivity. Debye relaxation model and its variants are popular models for biological media. In this relaxation model, the relative permittivity of the medium is expressed as [16]:

$$\epsilon_r(\omega) = \epsilon_\infty + \frac{\epsilon_{r0} - \epsilon_\infty}{1 - i\omega\tau} + i\frac{\sigma}{\omega\epsilon_0} \tag{29}$$

The imaginary component of $\epsilon_r(\omega)$ includes the static conductivity σ. That is, the dielectric loss in this model includes both relaxation loss and induced-current loss. In the expression, ϵ_∞ is the relative permittivity at frequencies where $\omega\tau \gg 1$, while ϵ_{r0} is the relative permittivity at $\omega\tau \ll 1$. This model is valid for frequency much less than $1/\tau$. For example, over the frequency range of 2.8 MHz $\ll f \ll$ 140 GHz, the parameters for muscle are: τ = 7.23 ps, $\epsilon_\infty = 4$, and $\epsilon_{r0} = 54$. Here, ϵ_∞ is the relative permittivity at 140 GHz or beyond, ϵ_{r0} is the relative permittivity at 2.8 MHz, and the relaxation model is valid for frequency much less than $1/\tau = 140 \times 10^9$ Hz.

In frequency region where $\omega\tau \ll 1$, the relative permittivity is approximately equal to

$$\epsilon_r(\omega) \approx \epsilon_{r0} + \frac{i}{\omega\epsilon_0}\big(\sigma + \omega^2\tau\epsilon_0\Delta\epsilon\big) \tag{30}$$

where $\Delta\epsilon = \epsilon_{r0} - \epsilon_\infty$. This yields

$$k_I \approx \frac{\sigma + \omega^2\tau\epsilon_0\Delta\epsilon}{2}\sqrt{\frac{\mu_0}{\epsilon_0\epsilon_{r0}}} \qquad |k| \approx \omega\sqrt{\mu_0\epsilon_0\epsilon_{r0}} \tag{31}$$

Now, k_I increases slowly with frequency. The asymptotic efficiency can be obtained from (28) by the following substitutions: $\epsilon_r \to \epsilon_{r0}$ and $\sigma \to \sigma + \omega^2\tau\epsilon_0\Delta\epsilon$. Defining $k_{I0} = \frac{\sigma}{2}\sqrt{\frac{\mu_0}{\epsilon_0\epsilon_{r0}}}$, the asymptotic optimal efficiency can be written as

$$\begin{aligned}\eta_{opt} = \frac{3k_{I0}e^{-2k_{I0}d_2}A^2/Z}{2\pi\sigma d_2^4}\Big[\big(\frac{d_2^2\epsilon_{r0}}{c^2} + \frac{d_2\tau\Delta\epsilon}{c\sqrt{\epsilon_{r0}}}\big)\big(|\beta_{-1}|^2 + |\beta_1|^2\big)\omega^2 \\ + 4|\beta_0|^2 - |\beta_{-1}|^2 - |\beta_1|^2 + 2k_{I0}d_2\big(|\beta_{-1}|^2 + |\beta_1|^2\big)\Big]e^{-\frac{d_2\tau\Delta\epsilon}{c\sqrt{\epsilon_{r0}}}\omega^2} + o(1)\end{aligned} \tag{32a}$$

as $\omega \to \infty$. The asymptotic term is maximized when

$$\omega_{opt} = \sqrt{\frac{c\sqrt{\epsilon_{r0}}}{d_2\tau\Delta\epsilon} - \frac{4|\beta_0|^2 - |\beta_{-1}|^2 - |\beta_1|^2 + 2k_{I0}d_2\big(|\beta_{-1}|^2 + |\beta_1|^2\big)}{\big(\frac{d_2^2\epsilon_{r0}}{c^2} + \frac{d_2\tau\Delta\epsilon}{c\sqrt{\epsilon_{r0}}}\big)\big(|\beta_{-1}|^2 + |\beta_1|^2\big)}} \tag{33}$$

If the transmit-receive separation is less than 2.5 times of the low-frequency skin depth, that is, $2k_{I0}d_2 < 5$, the asymptotic optimal frequency will be lower-bounded by

$$\omega_{opt} > \sqrt{\frac{c\sqrt{\epsilon_{r0}}}{d_2\tau\Delta\epsilon} - \frac{\big(|\beta_{-1}|^2 + |\beta_1|^2\big)^{-1}}{\big(\frac{d_2^2\epsilon_{r0}}{c^2} + \frac{d_2\tau\Delta\epsilon}{c\sqrt{\epsilon_{r0}}}\big)}} \approx \sqrt{\frac{c\sqrt{\epsilon_{r0}}}{d_2\tau\Delta\epsilon}} \tag{34}$$

The approximation is due to $\frac{d_2^2\epsilon_{r0}}{c^2} \gg \frac{d_2\tau\Delta\epsilon}{c\sqrt{\epsilon_{r0}}}$ in general. Gabriel et al. have experimentally characterized dielectric properties of 17 different kinds of biological tissue [18][1]. Table 1 lists the approximated lower bound for the 17 different tissues assuming $d_2 = 1$ cm. All lower bounds are in the GHz-range. Consequently, *for any potential depth of implant inside the body, the asymptotic optimal frequency is around the GHz-range for small transmit and small receive sources.*

As muscle is the most widely reported tissue, let us take muscle as an example. We compute the exact optimal frequencies that maximize the efficiency given in (15) for different transmit-receive separations, and compare them with the approximate lower bound in (34). Fig. 2(a) shows these curves. The implant depth in the graph refers to $d_2 - d_1$. The

[1] The parameters in [18] are for the 4-term Cole-Cole model which is a variant of the Debye relaxation model. Conversion to the Debye relaxation model is as follows: $\tau = \tau_1$, $\epsilon_{r0} = \Delta\epsilon_1 + \epsilon_\infty$, and $\sigma = \sum_{n=2}^4 \frac{\epsilon_0\Delta\epsilon_n}{\tau_n} + \sigma_s$

Table 1: Summary of the approximate lower bound on the asymptotic optimal frequency for 17 different kinds of biological tissue, assuming $d_2 = 1$ cm.

Tissue type	Approximate lower-bound on f_{opt} (GHz/cm$^{-1/2}$)
Blood	3.54
Bone (cancellous)	3.80
Bone (cortical)	4.50
Brain (grey matter)	3.85
Brain (white matter)	4.23
Fat (infiltrated)	6.00
Fat (not infiltrated)	8.64
Heart	3.75
Kidney	3.81
Lens cortex	3.93
Liver	3.80
Lung	4.90
Muscle	3.93
Skin (dry)	4.44
Skin (wet)	4.01
Spleen	3.79
Tendon	3.17

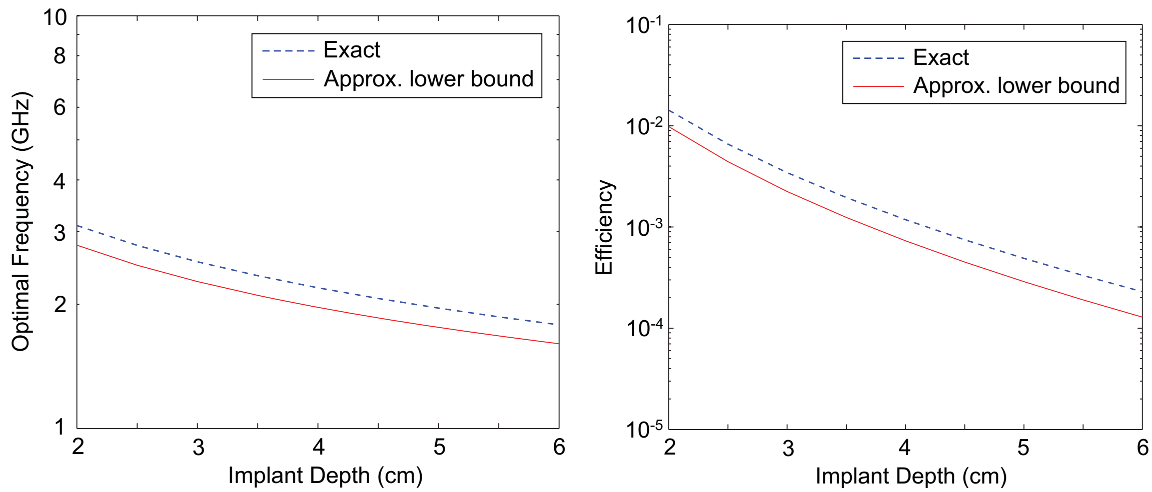

(a) (b)

Figure 2: Homogeneous medium – (a) optimal transmission frequency with $d_1 = 0.1d_2$ and receive coil tilted 45°; and (b) optimal efficiency with $A = (2\text{ mm})^2$ and $Z = 1\ \Omega$.

approximate lower bound is a good approximation to the exact value. As this lower bound is inversely proportional to $\sqrt{d_2}$, *the optimal frequency is approximately inversely proportional to* $\sqrt{d_2}$. In addition, we compute the exact optimal frequency using the multi-term Cole-Cole model [18], a variant of the Debye relaxation model that has a wider dielectric spectrum. The optimal frequencies are closer to the approximate lower bound.

Finally, the asymptotic term in (32) at $\omega = \omega_{opt}$ is lower-bounded by

$$\begin{aligned} \eta_{opt}^{as} &> \frac{3k_{I0}e^{-2k_{I0}d_2}A^2/Z}{2\pi\sigma d_2^4}\Big(\frac{d_2^2\epsilon_{r0}}{c^2} + \frac{d_2\tau\Delta\epsilon}{c\sqrt{\epsilon_{r0}}}\Big)\big(|\beta_{-1}|^2 + |\beta_1|^2\big)\frac{c\sqrt{\epsilon_{r0}}}{d_2\tau\Delta\epsilon}e^{-1} \\ &\approx \frac{3\sqrt{\mu_0/\epsilon_0}\epsilon_{r0}e^{-2k_{I0}d_2-1}A^2/Z}{4\pi c\tau\Delta\epsilon d_2^3}\big(|\beta_{-1}|^2 + |\beta_1|^2\big) \end{aligned} \tag{35}$$

Similarly, we compute the exact optimal efficiencies for different transmit-receive separations and compare them with the above approximate lower bound. Fig. 2(b) plots these two curves. The approximation shows good matches. Thus, *the optimal efficiency is approximately inversely proportional to (implant depth)*^{3}. In the far field, the power gain follows the inverse square law, that is, it is inversely proportional to the square of the transmit-receive separation. In the near field, the power gain is inversely proportional to the 6th power of the transmit-receive separation. Now, the optimal power transfer efficiency is somewhere in between the far field and the near field.

3.5 Trade-off between Receiver Miniaturization and Tissue Absorption

From (11) and (17), the tissue absorption can be written as

$$\begin{aligned} P_l = \frac{\omega\mu_0|k|^2 \operatorname{Im} k^2}{2}\Big\{&|\alpha_0|^2\Big[\frac{e^{-2k_I d_1}}{4k_I}\big(2 + k_I d_1 - 2k_I^2 k_1^2\big) + \frac{d_1 \mathrm{Ei}(-2k_I d_1)}{2}\big(3 - 2k_I^2 d_1^2\big)\Big] \\ &+ (|\alpha_{-1}|^2 + |\alpha_1|^2)\Big[\frac{e^{-2k_I d_1}}{8k_I}\big(4 - k_I d_1 + 2k_I^2 d_1^2\big) + \frac{d_1 \mathrm{Ei}(-2k_I d_1)}{4}\big(3 + 2k_I^2 d_1^2\big)\Big]\Big\} \\ &+ o(\omega^4) \end{aligned} \tag{36}$$

as $\omega \to \infty$. Therefore, P_l is approximately proportional to ω^4. Similarly, from (14) and (18), the received power can be written as

$$P_r = \frac{3\omega^2\mu_0^2|k|^4 A^2\, e^{-2k_I d_2}}{8\pi d_2^2 Z}\big|\alpha_{-1}\beta_{-1}^* + \alpha_1\beta_1^*\big|^2 + o(\omega^6) \tag{37}$$

as $\omega \to \infty$. Therefore, P_r is approximately proportional to $\omega^6 A^2$. Consequently, the efficiency is approximately proportional to $\omega^2 A^2$. If the transmission frequency is increased from 10 MHz to 1 GHz,

- the receive area will be reduced by 10^6 times for a fixed received power;
- the receive area will be reduced by 10^2 times for a fixed efficiency; and
- the efficiency will be increased by 10^4 times or 40 dB for a fixed receive area.

4 Point Source over Layered Medium

Conventional wisdom in wireless power transmission is to operate at lower frequency due to tissue absorption loss. Our analyses over homogeneous medium, however, bring out that the tissue absorption loss is not as worse as conventional wisdom believed. Next, we will investigate the effect of scattering from the layered nature of tissue on the optimal frequency.

We consider planar interfaces and magnetic dipoles as sources (see Fig. 3). As the electric and the magnetic fields are given in the form of Sommerfeld integrals [19, Sec. 2.3] and we need to compute the fields near the sources, closed-form analyses as in the homogeneous medium are not feasible. Alternately, we consider a multi-layer tissue model as illustrated in Fig. 3 and numerically compute the Sommerfeld integrals. To accelerate the computation, we follow [20] to deform the integration path. Furthermore, as the integrals involve Bessel

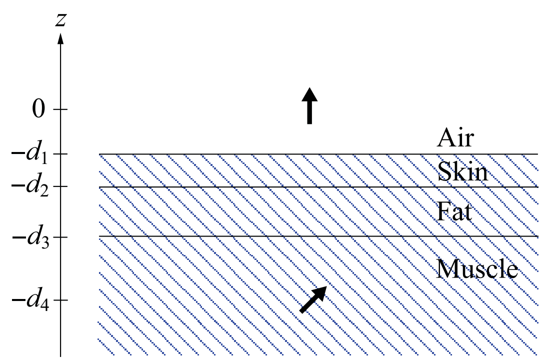

Figure 3: A magnetic dipole on top of a multi-layer interface with the receive coil embedded in the muscle layer.

functions which are oscillatory, we partition the revised integration path into sub-paths with exponentially increasing length, and perform the integration over these sub-paths.

Fig. 4(a) plots the optimal frequency versus the implant depth for both air-muscle half space and air-skin-fat-muscle multi-layer interface. In the latter case, the thickness of skin is 4.5 mm and the thickness of fat is 7.5 mm, that is, $d_2 - d_1 = 4.5$ mm and $d_3 - d_2 = 7.5$ mm. The receive coil is tilted 45° with respect to the interface which is equivalent to setting $(\beta_{-1}, \beta_0, \beta_1) = (1/2, \sqrt{1/2}, 1/2)$. Note that in the previous section, the receiver is at $-\hat{\mathbf{z}}d_2$ while in the multi-layer tissue model, it is at $-\hat{\mathbf{z}}d_4$.

The optimal frequencies are less than those obtained assuming homogeneous medium. This is due to the scattering from the interfaces. Optimal frequencies are relatively invariant with implant depth, particularly in the multi-layer case. The optimal frequency for the air-muscle half space is around 2 GHz and that for the multi-layer interface is around 1 GHz. That is, the optimal frequencies remain in the GHz-range. In addition, we compute the optimal frequencies for various receive coil orientation, and find out that the optimal frequencies are insensitive to the orientation which agrees with the prediction from (34).

Finally, we study how tissue interfaces affect the power transfer efficiency. Fig. 4(b) plots the optimal efficiency versus the implant depth in the 3 different media. Scattering by interfaces reduces the efficiency by almost an order of magnitude. The efficiency is slightly better with more layers because scattering reduces tissue absorption more than received power. The variation of the optimal efficiency with the implant depth, however, remains

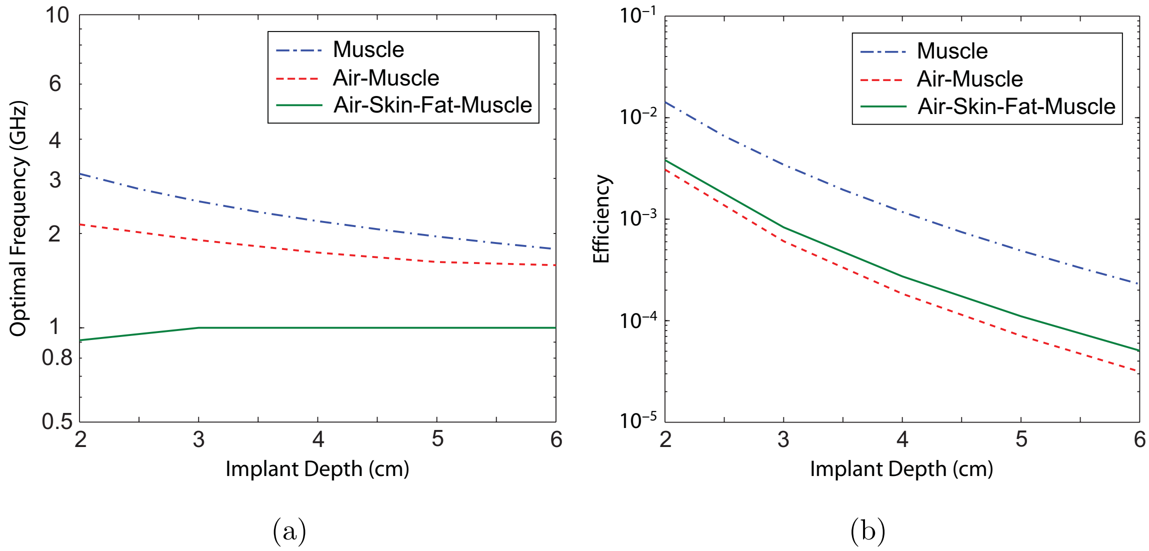

Figure 4: Inhomogeneous medium – (a) optimal transmission frequency with $d_1 = 0.1d_4$ and receive coil tilted 45°; and (b) optimal efficiency with $A = (2\text{ mm})^2$ and $Z = 1\ \Omega$.

approximately inversely proportional to (implant depth)^3.

In conclusion, both received power and tissue absorption increase with frequency. At a given frequency, tissue interfaces reduce both received power and tissue absorption; however, their ratio remains increasing with frequency initially. At the optimal frequency, the dispersiveness of tissue dominates. The received power begins decreasing with increasing frequency. Frequencies where tissue dispersiveness dominates, do not affect significantly by the tissue interfaces. As a result, the conclusion on the optimal frequency for point sources derived assuming homogeneous medium remains valid.

5 Finite Coil over Layered Medium

The analytical results and numerical examples presented are based on point sources. We will verify the result using finite coils through electromagnetic simulations. To explain the simulation results, we need to introduce the equivalent circuit for the power transmission link first.

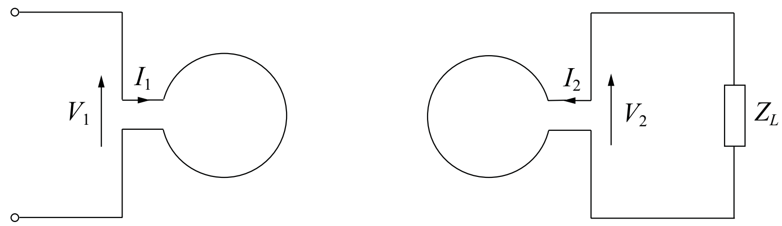

Figure 5: A single transmit and a single receive coil system

5.1 Equivalent Circuit Model

The mutual interaction between the two coils in Fig. 5 can be described by the impedance equations:

$$V_1 = Z_{11}I_1 + Z_{12}I_2$$

$$V_2 = Z_{21}I_1 + Z_{22}I_2$$

When the load impedance Z_L is conjugate matched to Z_{22},

$$I_2 = -\frac{Z_{21}}{Z_{22} + Z_L} = -\frac{Z_{21}}{2R_{22}} I_1$$

where R_{nm} is the real part of Z_{nm} for all n, m. In terms of the circuit parameters, the received power P_r, the tissue absorption P_l, and the efficiency defined earlier can be expressed as

$$P_r = \frac{1}{2} \operatorname{Re} Z_L |I_2|^2 = \frac{|Z_{21}|^2}{8R_{22}} |I_1|^2 \qquad P_l = \frac{1}{2}(R_{11} - R_w)|I_1|^2 \qquad \eta = \frac{|Z_{21}|^2}{4(R_{11} - R_w)R_{22}} \quad (38)$$

where R_w is the wire resistance of the transmit coil. The analytical results and numerical examples presented in the previous two sections are based on point sources and therefore, they do not include the ohmic loss in both coils. Furthermore, they do not take into account the scattered field from the receive coil when deriving the electromagnetic fields in (10).

When we take into account both ohmic loss and scattered field from the receive coil, we consider the input power to the system

$$P_{in} = \frac{1}{2} \operatorname{Re}(V_1 I_1^*) = \frac{1}{2} \operatorname{Re}\Big(Z_{11} - \frac{Z_{12}Z_{21}}{Z_{22} + Z_L}\Big)|I_1|^2 = \frac{1}{2}\Big[R_{11} - \frac{\operatorname{Re}(Z_{12}Z_{21})}{2R_{22}}\Big]|I_1|^2 \qquad (39)$$

The difference $P_{in} - P_r$ is the total dissipation power which includes tissue absorption due to the sum of incident field from the transmit coil and the scattered field from the receive coil, and ohmic loss in both coils. In the following, we will find the transmission frequency that maximizes $\frac{P_r}{P_{in}-P_r}$. This is equivalent to maximize the power gain of the system

$$G = \frac{P_r}{P_{in}} = \frac{|Z_{21}|^2}{4R_{11}R_{22} - 2\,\mathrm{Re}(Z_{12}Z_{21})} \tag{40}$$

Comparing the efficiency define in (38) and the power gain in (40), they are the same when $R_w, Z_{12}, Z_{21} \to 0$. This is equivalent to having negligible ohmic loss and negligible scattered fields.

Finally, we relate the mutual impedance Z_{21} to the field quantities and obtain an expression for Z. From definition, we have

$$Z_{21}I_1 = i\omega\mu_0 A\,\mathbf{H}(-\hat{\mathbf{z}}d) \cdot \hat{\mathbf{n}} \tag{41}$$

Comparing the P_r given in (8) with that in (38), we obtain

$$Z = 4R_{22} \tag{42}$$

The value of Z assumed in the numerical examples shown in Fig. 2 and 4 is equivalent to a receive coil of self impedance 0.25 Ω. Next, we will obtain its actual value through electromagnetic simulations.

5.2 Simulation Results

We use Zeland IE3D full-wave electromagnetic field solver [15] to obtain the S-parameters of the 2-port system in Fig. 6. The frequency dependence of the tissue dielectric properties are imported to the simulator according to the dielectric model in [18]. In the simulation, both transmit and receive coils are single-turn, 2-mm side square copper loops with a trace width of 0.20 mm and trace thickness of 0.04 mm. The transmit coil is in parallel with the tissue interfaces while the receive coil is tilted. Both coils are axially aligned.

Fig. 7(a) plots the variation of optimal frequency with implant depth. The optimal frequencies are slightly higher than those obtained assuming point sources, and remain in the GHz-range. At the optimal frequencies, R_{22} takes the value of 3.65 Ω at implant depth of 2 cm to 3 cm and 2.07 Ω at implant depth of 4 cm to 6 cm. Therefore, the respective actual values of Z are 14.6 Ω and 8.28 Ω. Fig. 7(b) plots the optimal power gain

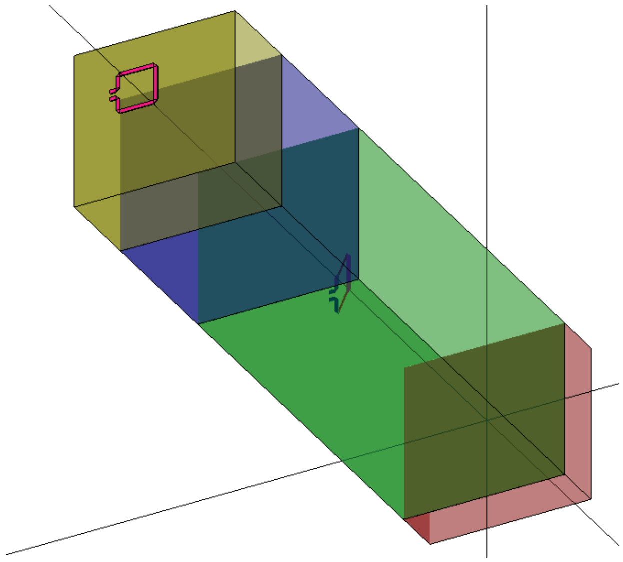

Figure 6: 3D view of the transmit coil, the receive coil, and the tissue model in IE3D

obtained from electromagnetic simulation as well as the optimal efficiency obtained from point-source analysis using the actual values of Z. The curve obtained from point-source analysis is slightly higher than the simulated one. This could be because the point-source analysis does not include the scattered field from the receiver and the ohmic loss in both coils. In conclusion, the point-source analysis is a good approximation when both transmit and receive coils are small.

For a pair of single-turn 2 mm×2 mm transmit and receive coils with a separation of 2 cm, the optimal power gain is about -40 dB. The gain is seemingly low; however, when we compare it with the normalized power gain[2] derived in [5] based on inductive coupling and shown in Table 2, the optimal power gain obtained from our full-wave analysis is far much better. In our example system, the magnitude of the mutual impedance at the optimal frequency is 0.0265 Ω which is equivalent to a mutual inductance of 0.0032 nH. Case 5 in Table 2 has similar mutual inductance where the power gain is -75 dB at 20 MHz and -77 dB at 2 MHz. By operating at the optimal frequency in the GHz-range, the power gain

[2] We normalize the power gain and the mutual inductance in [5] to a single-turn transmit and single-turn receive coils. This is done by dividing the power gain by the square of the number of turns in the receive coil, and dividing the mutual inductance by the product of the number of turns in the receive coil and that in the transmit coil.

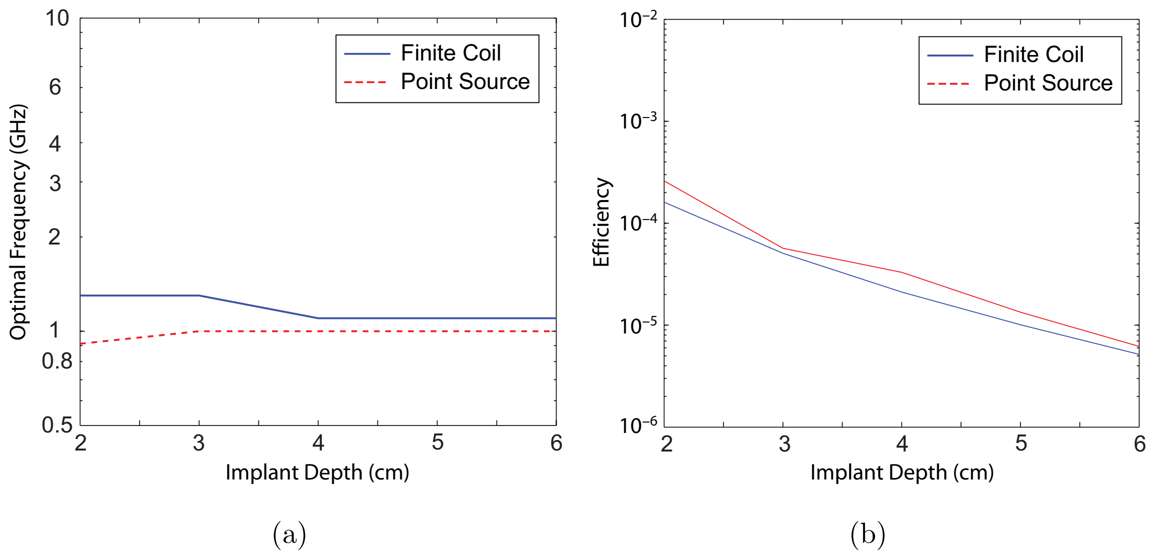

Figure 7: Electromagnetic simulation – (a) optimal transmission frequency versus implant depth and (b) optimal power gain or efficiency versus implant depth with $d_1 = 0.1d_4$, 2 mm$\times$2 mm transmit coil and receive coil, and receive coil tilted 45°.

is improved by more than 30 dB. Finally, reference [5] is a widely cited article on wireless powering of millimeter and sub-millimeter-sized implants. Our contribution in this paper is to prove that wireless power transmission for area-constrained implants can be operated at much higher frequency and can attain orders of magnitude improvement in the power transfer efficiency.

5.3 Transmit Dimension

The analytical results and the numerical examples in the previous two sections are based on point sources, and the dimension of the coils used in the electromagnetic simulations are small as well. These are justified at the receiver due to its area constraint. This constraint is lax at the transmitter. Using a larger transmit coil will shift the optimal frequency. Now, we replace the 2-mm width transmit coil by a 1-cm width coil and repeat the simulation. Fig. 8 plots the optimal frequency and the corresponding power gain versus the implant depth for two different orientations of the receive coil. The solid lines correspond to when the receive coil is in parallel with the transmit coil, and the dotted lines correspond to when the receive coil is tilted 45° with respect to the transmit coil. The optimal frequency

Table 2: Summary of normalized power gain G and normalized mutual inductance M for the five examples in [5].

Case	Freq.	A_t (mm^2)	A_t (mm^2)	M (nH)	G (dB)
1a	2 MHz	6.36×10^3	1.77	0.0250	-62.61
1b	20 MHz	6.36×10^3	1.77	0.0247	-61.58
2a	2 MHz	6.36×10^3	1.77	0.1238	-55.67
2b	20 MHz	6.36×10^3	1.77	0.1233	-54.59
3a	2 MHz	80.43×10^3	3.14	0.0167	-73.13
3b	20 MHz	80.43×10^3	3.14	0.0167	-71.76
4a	2 MHz	15.39×10^3	0.13	0.0008	-83.80
4b	20 MHz	15.39×10^3	0.13	0.0008	-82.04
5a	2 MHz	15.39×10^3	0.13	0.0041	-76.53
5b	20 MHz	15.39×10^3	0.13	0.0042	-74.96

decreases and varies from 0.5 GHz to 0.7 GHz – the sub-GHz range. In the sub-GHz range, the receiver remains not in the near field and therefore, we would expect the power gain to be less sensitive to receive coil orientation. This is confirmed by the curves in Fig 8(b) where the power gain is basically the same in both orientations. Finally, the power gain increases to -27 dB (about 0.2% efficiency) at the implant depth of 2 cm.

6 Conclusions

Wireless interfaces provide a convenience means of contactless monitoring of physiological processes. Its application to implantable medical devices is anticipated to be increasingly significant. To fully integrate the wireless interface with the rest of the implant circuits demands the use of small receive coils, for example, a millimeter-sized receive coil with centimeter range. In contrast to existing solutions being exclusively operated in the MHz-range, we show that the optimal transmission frequency is in the GHz-range for small transmit coils and in the sub-GHz range for larger transmit coils. That is, the optimal frequency is about 2 order of magnitude higher than existing solutions. For a fixed received power, the receive area can be reduced by 10^6 times. For a fixed receive area, the efficiency

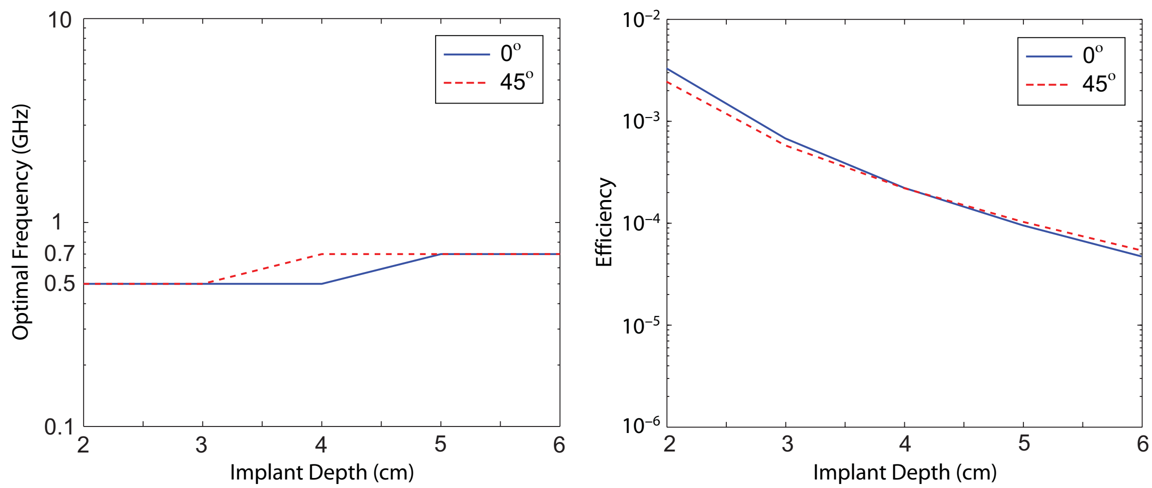

(a) (b)

Figure 8: Electromagnetic simulation – (a) optimal transmission frequency versus implant depth and (b) optimal power gain versus implant depth with $d_1 = 0.1d_4$, 1 cm×1 cm transmit coil, and 2 mm×2 mm receive coil.

can be improved by 30 dB including the scattering loss from tissue interfaces. For a fixed efficiency, the receive area can be reduced by 100 times. In addition, operating at higher frequency desensitizes the effect of receive coil orientation as now it is no longer in the near field of the transmitter. To exploit these advantages require new models and new circuit design techniques which can be the directions for future research in this area.

Acknowledgment

The authors would like to thank Professor Weng-Cho Chew of the University of Illinois at Urbana-Champaign for the useful discussions and valuable comments.

A Proof of (15)

Defining

$$\bar{\mathbf{A}} = \begin{bmatrix} \left|\mathbf{N}_{1,-1}(-\hat{\mathbf{z}}d_2)\right| & 0 & 0 \\ 0 & \left|\mathbf{N}_{1,0}(-\hat{\mathbf{z}}d_2)\right| & 0 \\ 0 & 0 & \left|\mathbf{N}_{1,1}(-\hat{\mathbf{z}}d_2)\right| \end{bmatrix}$$

$$\bar{\mathbf{B}} = \begin{bmatrix} \int_{\text{tissue}}\left|\mathbf{M}^{(3)}_{1,-1}(\mathbf{r})\right|^2 d\mathbf{r} & 0 & 0 \\ 0 & \int_{\text{tissue}}\left|\mathbf{M}^{(3)}_{1,0}(\mathbf{r})\right|^2 d\mathbf{r} & 0 \\ 0 & 0 & \int_{\text{tissue}}\left|\mathbf{M}^{(3)}_{1,1}(\mathbf{r})\right|^2 d\mathbf{r} \end{bmatrix}$$

and

$$\boldsymbol{\alpha} = \begin{bmatrix} \alpha_{-1} \\ \alpha_0 \\ \alpha_1 \end{bmatrix} \qquad \boldsymbol{\beta} = \begin{bmatrix} \beta_{-1} \\ \beta_0 \\ \beta_1 \end{bmatrix}$$

the efficiency can be written as

$$\eta = \frac{|k|^2 A^2/Z}{\operatorname{Im} k^2/(\omega\mu_0)} \frac{\left|\boldsymbol{\beta}^\dagger \bar{\mathbf{A}} \boldsymbol{\alpha}\right|^2}{\boldsymbol{\alpha}^\dagger \bar{\mathbf{B}} \boldsymbol{\alpha}}$$

Now we want to find $\boldsymbol{\alpha}$ to maximize η. As $\bar{\mathbf{B}}$ is positive definite, the optimal $\boldsymbol{\alpha}$ is

$$\boldsymbol{\alpha}_{opt} = \bar{\mathbf{B}}^{-1}\bar{\mathbf{A}}\boldsymbol{\beta}$$

which yields

$$\eta_{opt} = \frac{|k|^2 A^2/Z}{\operatorname{Im} k^2/(\omega\mu_0)} \boldsymbol{\beta}^\dagger \bar{\mathbf{A}}\bar{\mathbf{B}}^{-1}\bar{\mathbf{A}}\boldsymbol{\beta}$$

References

[1] J. C. Schuder, H. E. Stephenson, Jr., and J. F. Townsend, "High-level electromagnetic energy transfer through a closed chest wall," *IRE Intl. Conv. Rec*, vol. 9, pp. 119–126, 1961.

[2] J. C. Schuder, J. H. Gold, H. Stoeckle, and J. A. Holland, "The relationship between the electric field in a semi-infinite conductive region and the power input to a circular coil on or above the surface," *Med. Biol. Eng.*, vol. 14, no. 2, pp. 227–234, Mar. 1976.

[3] F. C. Flack, E. D. James, and D. M. Schlapp, "Mutual inductance of air-cored coils: effect on design of radio-frequency coupled implants," *Med. Biol. Eng.*, vol. 9, no. 2, pp. 79–85, Mar. 1971.

[4] D. C. Galbraith, "An implantable multichannel neural stimulator," Ph.D. dissertation, Stanford University, Dec. 1984.

[5] W. J. Heetderks, "RF powering of millimeter- and submillimeter-sized neural prosthetic implants," *IEEE Trans. Biomed. Eng.*, vol. 35, no. 5, pp. 323–327, May 1988.

[6] W. H. Ko, S. P. Liang, and C. D. Fung, "Design of radio-frequency powered coils for implant instruments," *Med. Biol. Eng. Comp.*, vol. 15, pp. 634–640, 1977.

[7] I. C. Forster, "Theoretical design and implementation of transcutaneous multichannel stimulator for neural prostheses applications," *J. Biomed. Eng.*, vol. 3, pp. 107–120, April 1981.

[8] N. de N. Donaldson and T. A. Perkins, "Analysis of resonant coupled coils in the design of radio-frequency transcutaneous links," *Med. Biol. Eng. Comput.*, vol. 21, pp. 612–627, Sept. 1983.

[9] E. S. Hochmair, "System optimization for improved accuracy in transcutaneous signal and power transmission," *IEEE Trans. Biomed. Eng.*, vol. 31, pp. 177–186, Feb. 1984.

[10] P. E. K. Donaldson, "Frequency-hopping in R.F. energy-transfer links," *Electron. Wireless World*, pp. 24–26, Aug. 1986.

[11] C. M. Zierhofer and E. S. Hochmair, "High-efficiency coupling-insensitive transcutaneous power and data transmission via an inductive link," *IEEE Trans. Biomed. Eng.*, vol. 37, no. 7, pp. 716–722, July 1990.

[12] ——, "Geometric approach for coupling enhancement of magnetically coupled coils," *IEEE Trans. Biomed. Eng.*, vol. 43, no. 7, pp. 708–714, July 1996.

[13] T. Akin, K. Najafi, and R. M. Bradley, "A wireless implantable multichannel digital neural recording system for a micromachined sieve electrode," *IEEE J. Solid-State Circuits*, vol. 33, no. 1, pp. 109–118, Jan. 1998.

[14] W. Liu, K. Vichienchom, M. Clements, S. C. DeMarco, C. Hughes, E. McGucken, M. S. Humayun, E. de Juan, J. D. Weiland, and R. Greenberg, "A neuro-stimulus chip with telemetry unit for retinal prosthetic device," *IEEE J. Solid-State Circuits*, vol. 35, no. 10, pp. 1487–1497, Oct. 2000.

[15] Zeland Software Inc., "IE3D version 12.2."

[16] A. V. Vorst, A. Rosen, and Y. Kotsuka, *RF/Microwave Interaction with Biological Tissues*. New Jersey, USA: Wiley-IEEE Press, 2006.

[17] J. D. Jackson, *Classical Electrodynamics*, 3rd ed. Wiley, 1998.

[18] S. Gabriel, R. W. Lau, and C. Gabriel, "The dielectric properties of biological tissues: III. parametric models for the dielectric spectrum of tissues," *Phys. Med. Biol.*, vol. 41, no. 11, pp. 2271–2293, Nov. 1996.

[19] W. C. Chew, *Waves and Fields in Inhomogeneous Media*. IEEE Press, 1995.

[20] T. J. Cui and W. C. Chew, "Fast evaluation of Sommerfeld integrals for EM scattering and radiation by three-dimensional buried objects," *IEEE Trans. Geosci. Remote Sensing*, vol. 37, no. 2, pp. 887–900, Mar. 1999.